Published in final edited form as:
Dev Neurobiol. 2012 August ; 72(8): 1161–1179. doi:10.1002/dneu.22006.

Structure-Function Analysis of Endogenous Lectin Mind-the-Gap in Synaptogenesis

Emma Rushton, **Jeffrey Rohrbough**, **Kalie Deutsch**, and **Kendal Broadie***
Department of Biological Sciences, Kennedy Center for Research on Human Development, Vanderbilt University, Nashville, TN 37232, USA

Abstract

Mind-the-Gap (MTG) is required for neuronal induction of *Drosophila* neuromuscular junction (NMJ) postsynaptic domains, including glutamate receptor (GluR) localization. We have previously hypothesized that MTG is secreted from the presynaptic terminal to reside in the synaptic cleft, where it binds glycans to organize the heavily-glycosylated, extracellular synaptomatrix required for *trans*-synaptic signaling between neuron and muscle. In this study, we test this hypothesis with MTG structure-function analyses of predicted signal peptide (SP) and carbohydrate-binding domain (CBD), by introducing deletion and point-mutant transgenic constructs into *mtg* null mutants. We show that the SP is required for MTG secretion and localization to synapses *in vivo*. We further show that the CBD is required to restrict MTG diffusion in the extracellular synaptomatrix and for postembryonic viability. However, CBD mutation results in elevation of postsynaptic GluR localization during synaptogenesis, not the *mtg* null mutant phenotype of reduced GluRs as predicted by our hypothesis, suggesting that proper synaptic localization of MTG limits GluR recruitment. In further testing CBD requirements, we show that MTG binds N-acetylglucosamine (GlcNAc) in a Ca^{2+}-dependent manner, and thereby binds HRP-epitope glycans, but that these carbohydrate interactions do not require the CBD. We conclude that the MTG lectin has both positive and negative binding interactions with glycans in the extracellular synaptic domain, which both facilitate and limit GluR localization during NMJ embryonic synaptogenesis.

Keywords

synaptomatrix; glycan; carbohydrate-binding domain; neuromuscular junction; *Drosophila*

INTRODUCTION

Carbohydrate-binding lectins are best known as plant-derived research tools, initially as hemagglutination and immunological reagents, and later in neuroscience as classic synaptic markers (Ribera et al., 1987; Scott et al., 1988; Iglesias et al., 1992) and *trans*-synaptic tracers (Gonatas et al., 1979; Itaya and van Hoesen, 1982; Fabian and Coulter, 1985). The broad spectrum of plant lectin proteins exhibit a range of carbohydrate-binding specificity, which as synaptic markers have revealed the unique character of the carbohydrate landscapes on pre- and postsynaptic membranes, and within the surrounding extracellular synaptomatrix (Broadie et al., 2011; Dani and Broadie, 2011). For example, studies at the rat neuromuscular junction (NMJ) synapse using *Dolichos biflorus*, *Glycine max* and *Vicia villosa* lectins show highly specific glycan expression patterns owing to oligosaccharide N-

*Correspondence: Kendal Broadie, VU Station B, Box 35-1634, Nashville, Tennessee 37235-1634, USA Phone: (615) 936-3937, Fax: (615) 936-0129, kendal.broadie@vanderbilt.edu.

acetylgalactosaminyl termini (Sanes and Cheney, 1982). Later studies (Martin and Sanes, 1995) showed that the *Vicia villosa* lectin has biological activity, promoting acetylcholine receptor (AChR) clustering and potentiating the synaptogenic activity of the classical Agrin proteoglycan. Indeed, Agrin itself is one of a large and growing list of endogenous lectins, including the neural pentraxins involved in AMPA glutamate receptor (GluR) clustering (O'Brien et al., 1999; Zhou et al., 2001; O'Brien et al., 2002), and the lecticans aggrecan, brevican, versican and neurocan, members of the large and diverse C-lectin family involved in synapse formation, function and plasticity (Aspberg et al., 1997; Hagihara et al., 1999; Yamagata and Sanes, 2005; Xiang et al., 2006). Agrin has a glycan-binding lectin domain important for NMJ development (Rupp et al., 1991; Tsim et al., 1992; Tsen et al., 1995). Perturbation of synaptic glycosaminoglycans (GAGs) interferes with the Agrin signaling that drives AChR cluster maintenance (McDonnell and Grow, 2004). Moreover, Gal(β1,4)GlcNAc and Gal(β1,3)GalNAc glycans similarly inhibit Agrin signaling by suppressing muscle specific kinase (MuSK) autophosphorylation, a key step during NMJ synaptogenesis (Parkhomovskiy et al., 2000).

Both O- and N-linked glycosylation are likewise important at the *Drosophila* NMJ, a well-characterized model glutamatergic synapse (Broadie et al., 2011). Mutations of *POMT1/2* (dolichyl-phosphate-mannose-protein mannosyltransferase 1 and 2) disrupt O-glycosylation, particularly of the proteoglycan Dystroglycan (Dg) ECM receptor, reducing both postsynaptic GluR number and presynaptic vesicular glutamate release (Wairkar et al., 2008). Mutation of *Mgat1* (UDP-GlcNAc: a-3-D-mannoside-β1,2-N-acetylglucosaminyltransferase I, also known as GlcNAcT1) disrupts the N-glycosylation of numerous synaptic proteins, and results in abnormal neural development, locomotory defects and shortened lifespan due to a *Mgat1* requirement in neurons (Sarkar et al., 2006; Sarkar et al., 2010). The *mind-the-gap (mtg)* gene encodes a predicted endogenous lectin that localizes at the *Drosophila* NMJ, and is required for formation of the electron-dense, heavily-glycosylated synaptomatrix between presynaptic active zones and postsynaptic GluR domains (Rohrbough et al., 2007). MTG induces synaptic localization of GluRs and other postsynaptic domain proteins, including glycoprotein integrin ECM receptors, and modulates the *trans*-synaptic signaling of presynaptically secreted Jelly Belly (Jeb) ligand to glycoprotein Alk postsynaptic receptor (Rushton et al., 2009; Rohrbough and Broadie, 2010). Neuronally-targeted MTG expression alters the NMJ glycan landscape, as assayed with *Vicia villosa* and wheat germ agglutinin lectins (Rushton et al., 2009). MTG contains a predicted signal peptide (SP) hypothesized to be required for presynaptic secretion, and a predicted carbohydrate-binding domain (CBD) hypothesized to bind N-acetylglucosamine (GlcNAc) moieties on synaptic cleft N-glycans to regulate NMJ synaptogenesis (Rushton et al., 2009).

In this study, we first perform a MTG structure-function analysis, focusing on the SP and CBD to test the above two hypotheses. Transgenic constructs of wildtype MTG or mutant MTG lacking one of these domains were expressed in neurons to assay the effect on protein trafficking and distribution. Expression in otherwise *mtg* null mutant animals was used to assess neuronal functions *in vivo*. We show that the SP is required for MTG secretion and the extracellular localization of MTG at the NMJ synapse. We show that the CBD is required for viability; wildtype MTG rescues *mtg* null animals to adulthood, but null mutants expressing MTG lacking the CBD either fail to hatch or immediately die as very young postembryonic animals. Moreover, elimination of the CBD results in increased migration of secreted MTG from presynaptic terminals, expanding the extracellular localization of the protein. We have previously shown that wildtype MTG rescues *mtg* null synaptic defects including loss of GluR localization and NMJ postsynaptic function (Rushton et al., 2009; Rohrbough and Broadie, 2010). Unexpectedly, MTG lacking the CBD also restores normal embryonic NMJ postsynaptic function and rescues the loss of GluR

localization in *mtg* null mutants. Indeed, lack of the CBD leads to increased postsynaptic GluR accumulation compared to rescue with wildtype MTG, demonstrating a MTG inhibitory function. A likely explanation for these results is the unexpected finding that the CBD is not required for the Ca^{2+}-dependent binding of MTG to GlcNAc or glycans, resembling similar findings for mammalian C-lectin family members (lecticans) (Aspberg et al., 1997). These findings suggest that the CBD has a regulatory role in MTG function, rather than acting as the primary carbohydrate-binding domain. Taken together, these data show that secreted MTG has both positive and negative glycan interactions within the synaptomatrix, which both facilitate and limit GluR localization during embryonic synaptogenesis at the NMJ.

METHODS

Generation of *mtg* mutant transgenic constructs

The *mtg* coding sequence was amplified using paired forward and reverse primers: CACCATGAACTTTTTTGTGATTGGCTTTCTG and GTTGGATAGCTGCTGCTCTG. For the SP deletion construct, the forward primer was CACCATGGCTTGCGGGACG. PCR products were cloned into pENTR vector (Gateway, Invitrogen) to make pENTR-MTG and pENTR-ΔSP-MTG, and confirmed by sequencing (Fig. 1A). The ΔCBD mutant construct was made by cutting pENTR-MTG with HindIII and SacI, and re-ligating to make an in-frame deletion of the entire CBD (Fig. 1A). CBD point mutations were introduced using the Gene Tailor kit (Invitrogen) with the following primers: C2-3, ACGCTGACACCGACCTTGGCGCCATGGTATTCCACGTAGCCGCCCTAAC (forward) and GCCAAGGTCGGTGTCAGCGTAGAGACCGGG (reverse); C5-6, TCGACCAGACG ATCTTAAAGGCCAACTGGTGGTTCTACGTCGACGCCAGCTCTAG (forward) and CT TTAAGATCGTCTGGTCGAAGAGTGTGTTC (reverse); and FDIA CCGGAGAACACAC TCATCGCCCAGACGATC (forward) and GAAGTCGTTCCTTTGCCCGGAGAACACA CTC (reverse). Subsequently, each wildtype and mutant *mtg* construct was recombined into the vector pP{TWG} containing both a UAS promoter and a C-terminal GFP tag (*Drosophila* Genomics Resource Center).

Drosophila genetics

Background control w^{1118} embryos were injected with pP{TWG} MTG::GFP constructs (Genetics Services Inc.). Transformants were mapped and homozygous lines established using w^{1118} and w^{1118}; ap^{Xa}/CyO-MKRS. The *mtg* null stock used was mtg^{1}/TM3 Kr-GFP Sb^{1} (P{GAL4-Kr.C}DC2, P{UAS-GFP.S65T}DC10) (Rohrbough et al., 2007). UAS lines used include UAS-eGFP (P{w^{+mC}=UAS-EGFP}8, w^{1118} and UAS-P{TWG} wt-, ΔSP.ΔCBD-, C2-3-, C5-6- and FDIA-MTG::GFP (Fig. 1A). Ubiquitous expression of transgenic lines was driven using UH1-GAL4 (w^{1118}; P{GAL4-da.G32}UH1) (Rohrbough et al., 2004). Neuronal expression was driven using *elav*-GAL4 (P{GawB}$elav^{C155}$) (Fig. 1B,C) (Lin and Goodman, 1994; Rohrbough et al., 2004). For rescue experiments, mtg^{1} was recombined with third chromosome insertions of pP{TWG} UAS wt-MTG, ΔCBD- or C2-3 MTG::GFP. These stocks were crossed with UH1-gal4, mtg^{1}/TM3 Kr-GFP Sb^{1}. For GlcNAc binding assays, Western and Far-Western blots, the stocks used were *elav*-GAL4; UAS wt-MTG::GFP, *elav*-GAL4, UAS-eGFP and *elav*-GAL4; UAS-ΔCBD-MTG::GFP.

Viability assays

UH1-GAL4, mtg^{1}/TM3 Kr-GFP Sb^{1} females were crossed to UAS wildtype- or mutant MTG::GFP, mtg^{1}/TM3 Kr-GFP Sb^{1}. To assay embryo hatching and early larval viability, 100 embryos per trial were counted onto an apple juice/agar plate and allowed to develop for 24 hours at 25°C. Homozygous mtg^{1} animals were identified by absence of the

characteristic Kr-GFP balancer fluorescence. The number of unhatched embryos and dead larvae were counted. To assay adult viability, the number of adult animals with and without the Sb marker were counted. If the *mtg*^{1} null mutant was totally rescued, one third of adults would be expected to lack the Sb marker.

Immunocytochemisty

Staged 20–22 hr after egg laying (AEL) embryos were dechorionated in bleach, washed in dH_2O and transferred to low Ca^{2+} saline (in mM: 135 NaCl, 5 KCl, 4 $MgCl_2$, 0.2 mM $CaCl_2$, 5 TES, 75 Sucrose, 2 NaOH, pH 7.2). Embryos were genotyped based on the Kr-GFP balancer chromosome. Control, mutant and rescued embryos were processed and imaged together under identical conditions. Embryos were glued to sylgard-coated coverslips, dissected dorsally and glued flat as described previously (Featherstone et al., 2009; Rushton et al., 2009; Rohrbough and Broadie, 2010), fixed for 10–15 mins in 4% paraformaldehyde, and washed in PBS (Invitrogen) containing 0.1% triton-X-100 (TX, Fisher) for ≥1 hr. Wandering 3rd instar larvae were dissected in saline consisting of 128 mM NaCl, 2 mM KCl, 4 mM $MgCl_2$, 70 mM sucrose, 5 mM HEPES, pH 7.2, fixed 10 minutes in 4% paraformaldehyde in phosphate-buffered saline (PBS) (Invitrogen) and washed in PBS alone, or in PBS + 0.1% triton X-100. Subsequent washes and incubations took place in PBS with or without detergent. For embryo antibody labeling, preparations were incubated overnight at 4°C with rabbit anti-GluRIIC (1:500; kind gift of Aaron DiAntonio (Marrus et al., 2004)); or mouse anti-discs large (Dlg; 1:500; DSHB mAb 4F3 (Parnas et al., 2001)). Fluorescent Alexa-488 and AlexA-555 conjugated secondaries (1:500; Molecular Probes) and Cy5-conjugated goat anti-HRP (1:500; Jackson laboratories) were applied for 1.5–2.5 hrs at room temperature. MTG::GFP was visualized by native fluorescence or with FITC-conjugated anti-GFP (1:500; Abcam 6662). For larval antibody labeling, Cy3- or Cy5- goat anti-HRP (1:200; Jackson Laboratories), FITC goat anti-GFP 6662 (1:500; Abcam), mouse anti-discs large (Dlg; 1:500; DSHB mAb 4F3 (Parnas et al., 2001)). The secondary Alexa 546 goat anti-mouse (1:500; Invitrogen) was used. Images were acquired on a Zeiss 510 confocal microscope (40–63X oil objectives) using LSM acquisition software.

Image quantification

For embryo studies, confocal Z-axis projections of GluR and HRP double-labeled NMJs were acquired at segments A2–A4 at effective magnifications of 100–200X. Anti-GluR fluorescence was thresholded in ImageJ to outline localized synaptic ROI at NMJs 6/7, 13, 12, defined by proximity to the HRP-labeled presynaptic terminal at each NMJ. Synaptic ROI areas and mean intensities were measured individually, and in a pooled ROI combining NMJs 6/7, 13, and 12 for each imaged hemisegment. Quantified measurements of GluR fluorescence area and mean fluorescence intensity were normalized to control values in the same experiment. Matched control and mutant images were exported to Adobe photoshop for display, with any pixel level adjustments performed on the entire image set. For larvae studies, to quantify distance of MTG::GFP puncta from the presynaptic neural membrane, Z-stack images of the larval NMJ on muscle 4 were projected using Zeiss LSM software and opened in Metamorph software. The NMJ was outlined using a thresholding function in the HRP channel, and the line tool was used to measure nearest distance between the NMJ outline and puncta. Significance was calculated using the Kruskal-Wallis and Wilcoxon Rank Sum tests.

Electrophysiology

20–22 hr AEL embryos were genotyped and dissected as described above, then incubated for 45–90 sec in collagenase (1.0 mg/ml, Sigma type IV in 0.2 mM Ca^{2+}), and then washed with recording saline containing 1.8 mM Ca^{2+} (Featherstone et al., 2009). Whole-cell patch-clamp recordings were made at a muscle holding potential of -60mV from embryonic

muscle 6 in abdominal segments A2–A4, using an Axopatch 1D amplifier with PClamp7 acquisition and analysis software (Axon Instruments) (Rohrbough et al., 2007). Postsynaptic glutamate currents were elicited by brief iontophoretic application (5ms, −50V pulse) of 100 mM L-glutamate (pH 9–10 in dH_20) from sharp microelectrodes, positioned directly between muscles 6/7. Multiple (5–10) responses were elicited in each recording, with maximal response amplitudes used for quantification. Currents were sampled at 10 kHz and filtered at 1–2 kHz. Representative data records were exported for display using Excel and Kaleidagraph graphics software. One-way ANOVA and Dunnett multiple comparisons tests were used for all statistical comparisons between genotypes.

GlcNAc binding assays

Protein samples were prepared using 3rd instar salivary glands from animals expressing MTG::GFP, ΔCBD-MTG::GFP or eGFP. The tissue was ground in lysis buffer consisting of 20 mM sodium phosphate buffer, 100 mM NaCl, 2 mM dithiothreitol, 0.1 mM EDTA and Roche complete mini-protease. Lysates were centrifuged for 20 mins at 4°C, and supernatants applied to agarose beads alone, or to beads conjugated with N-acetyl glucosamine (GlcNAc) (Sigma) or to Chitin beads (GlcNAc polymer) (New England BioLabs). Samples were incubated for 2 hrs at room temperature, and then beads were washed in PBS to remove unbound proteins. Protein was eluted from the beads using 0.4 M GlcNAc in PBS. For Ca^{2+}-dependence experiments, PBS containing twice the final concentration of calcium was added to an equal volume of lysate before applying to the beads, and subsequent washes contained the same calcium concentration. For the Ca^{2+}-free condition, 2.5 mM EDTA was added to the lysate and washes.

Immunoprecipitation and Western Blots

Salivary gland lysates were incubated for 2 hrs at RT with Dynabeads (Invitrogen) cross-linked with anti-GFP (Abcam 6662), then washed with PBS to remove unbound proteins. For deglycosylation, the QA Bio Enzymatic CarboRelease Kit was used, including PNGaseF (N-glycans); O-glycosidase, Sialidase and β-Galactosidase; and Glucosaminidase (O-glycans). 5 gland lysates were incubated according to instructions, in the presence or absence of enzyme, and assayed by anti-GFP Western blot. For Western blots, lysates and beads were heated to 70°C for 10 mins with Nupage SDS sample buffer and run on 4–12% bis-tris SDS polyacrylamide gels (Invitrogen). Gels were stained using Colloidal Brilliant Blue (Invitrogen), or transferred to PVDF membranes stained using anti-GFP (Abcam 6662; 1:5000) or anti-HRP (Jackson Laboratory; 1:5000), followed by Alexa 680 anti-goat (1:5000; Invitrogen). All antibody dilutions for Western blots were in Odyssey buffer (LiCor), with membranes scanned on an Odyssey infrared imager (LiCor). For Far-Western blots, wildtype embryos were collected 12–22 hours AEL, bleached, rinsed and ground in lysis buffer. 10 μg of embryo lysate were diluted in NuPAGE sample buffer and loaded per lane. Wildtype head lysates were prepared by grinding in Laemmli's sample buffer (Bio-Rad). Samples were then separated by SDS-PAGE and transferred to PVDF membranes. Far Western probes were prepared as follows: 100 each of MTG::GFP and eGFP-expressing salivary glands were ground in lysis buffer and centrifuged as above. The resulting supernatant was diluted in 2.5 ml of Odyssey buffer and incubated on the membrane four hours 4°C. Binding was detected with anti-GFP (1:5000) followed by Alexa 680 anti-goat (1:5000). Membranes were also probed with Alexa 680 wheat germ agglutinin (WGA) (0.4 μg/ml; Invitrogen) and anti-HRP (1:5000; Jackson Laboratories).

RESULTS

Generation of MTG transgenic animals

MTG is an essential protein required for postsynaptic development and postembryonic viability (Rohrbough et al., 2007; Rushton et al., 2009; Rohrbough and Broadie, 2010). We have hypothesized that MTG is secreted from the presynaptic terminal to bind GlcNAc-containing glycans in the NMJ extracellular synaptomatrix to induce the localization of numerous postsynaptic proteins driving the formation of concentrated glutamate receptor (GluR) domains. In support of this hypothesis, MTG has a predicted signal peptide (SP) for secretion and a predicted carbohydrate-binding domain (CBD) for extracellular glycan interaction, as well as glutamine-rich, threonine-rich and coiled-coil domains of unknown significance (Fig. 1A). To study the role of the two domains with predicted functions, the SP and the CBD, targeted mutations were made in the *mtg* coding sequence. Mutant constructs include a deletion of the SP (ΔSP) and a deletion of the entire CBD (ΔCBD; Fig. 1A). To further dissect the role of the CBD, cysteine-to-alanine point mutations were made in conserved cysteine residues predicted to be essential for correct CBD folding (Rohrbough et al., 2007; Rushton et al., 2009). The C2-3 mutant alters the second and third cysteines, and the C5-6 mutant alters the fifth and sixth cysteines, respectively (Fig. 1A). The disulfide bridges have been determined for the CBD of tachycitin to be C1–C3, C2–C6 and C4–C5. Each point-mutation construct is therefore expected to disrupt two disulfide bridges forming the predicted MTG glycan-binding pocket (Kawabata et al., 1996; Shen and Jacobs-Lorena, 1999; Arakane et al., 2003). Finally, a conserved CBD phenylalanine-aspartate pair was mutated to isoleucine-alanine (FDIA). In total, six MTG variants were made for structure-function analyses; a full-length wildtype MTG and five different mutant variant constructs (Fig. 1A).

An important concern in any structure-function analyses is that the introduced structural changes might destabilize the protein, invalidating functional comparisons. Several tests were therefore conducted to compare expression levels and protein stability amongst the MTG mutant variants. First, wildtype and mutant MTG constructs were cloned into pP[AWM}, a Gateway tissue culture vector, which expresses MYC-tagged proteins under the actin5C promoter. The MTG mutant proteins are all synthesized and stably expressed in S2 cells at levels comparable to the wildtype protein. Confocal imaging of transformed S2 cells show an indistinguishable fluorescence level and pattern (data not shown). Likewise, Western blots show MTG proteins of the expected size, as recognized by the anti-MYC epitope tag, with the ΔCBD variant slightly smaller in molecular weight, as expected (data not shown). Second, protein expression was characterized *in vivo* in transgenic animals. Wildtype and mutant constructs were cloned into the Gateway pUAS-T expression vector pP{TWG}, upstream of a GFP epitope tag. The *elav*-Gal4 pan-neuronal driver was used for expression in the nervous system, including the wandering 3rd instar central nervous system ventral nerve cord (VNC; Fig. 1B) and peripheral neuromuscular junction (NMJ; Fig. 1C), as well as the salivary glands, a tissue specialized for high-level secretion. With the exception of ΔSP, mutant MTG proteins are all made and stably expressed in the salivary glands (Fig. 2A). ΔSP level appears strongly suppressed, consistent with a block of secretion (Fig. 2A, top middle). Also consistent with this result, the ΔSP protein alone is not detectable by salivary gland Western blot (data not shown), suggesting cells down-regulate MTG expression in response to accumulation of the non-secretable form. All of the CBD mutant proteins are synthesized at levels indistinguishable from wildtype control, and are similarly secreted to accumulate in the extracellular lumen (Fig. 2A). Surprisingly, as with wildtype MTG, all the CBD mutant proteins adhere on or near the surface of the secreting cells, implying that the CBD is not required for MTG binding to the glycosylated membrane or pericellular ECM. These data conclusively show that introduced CBD mutations do not

compromise protein expression and stability, allowing a detailed MTG structure-function comparison.

Expression of mutant forms of MTG at neuronal synapses

Wildtype MTG::GFP is efficiently trafficked to neuronal synapses, where it accumulates in the central synaptic neuropil (Fig. 1B) and at NMJ synaptic boutons (Fig. 1C) (Rohrbough et al., 2007; Rushton et al., 2009; Rohrbough and Broadie, 2010). To examine this neuronal trafficking and synaptic localization in the MTG mutant variants, *elav*-GAL4-driven MTG::GFP expression was assayed using anti-GFP, compared to the neural glycan marker anti-horse radish peroxidase (HRP). In the VNC, detergent was used in order to penetrate the VNC sheath and dense structure of the central neuropil, and to show the intracellular expression of MTG::GFP. Wildtype protein is observed in neuronal cell bodies and axons, where the protein is synthesized and transported, but particularly accumulated within the synaptic neuropil (np; Fig. 3). In contrast, the SP protein variant shows greatly reduced MTG::GFP expression in the VNC (left image shown at the same gain as WT MTG::GFP). When the imaging gain is increased (right image), a low level of ΔSP protein expression is observed exclusively in neuronal cell bodies, but with no detectable accumulation in the synaptic neuropil (Fig. 3). The low level of ΔSP protein expression implies it is downregulated in neurons, as in the salivary gland, when its introduction into the secretory pathway is prevented. Surprisingly, the fΔCBD protein also appears moderately downregulated compared to wildtype MTG::GFP, unlike in the salivary gland (Fig. 3, compare Fig. 2A). Overall, the ΔCBD protein expression pattern in neuronal cell bodies and synaptic neuropil closely resembles wildtype MTG, suggesting that the CBD is not required for neuronal intracellular trafficking, secretion or synaptic accumulation of MTG. The C2-3, C5-6 and FDIA CBD point mutant variants are likewise each expressed at yet lower levels within the VNC, but with expression patterns that resemble WT and CBD MTG (Fig. 3).

At the NMJ synapse, wildtype MTG::GFP is trafficked to presynaptic boutons and secreted into the extracellular space, where the protein is accumulated in puncta surrounding the nerve terminal (Fig. 1C). MTG mutant variants were compared with anti-GFP and anti-HRP co-labeling, in the absence of detergent to preserve and highlight extracellular MTG::GFP puncta (Fig. 2B). The ΔSP mutant protein is undetectable at NMJs or in the surrounding perisynaptic region. This is further evidence consistent with the requirement of the signal peptide for the vesicular axonal trafficking of MTG, and secretion by the nerve terminal into the synaptomatrix. In sharp contrast, the ΔCBD mutant protein is clearly expressed at the NMJ and secreted into the extracellular space surrounding the synaptic boutons (Fig. 2B). These findings are also consistent with the expectation that the CBD is not required for axonal transport or secretion into the ECM. Surprisingly, however, the C2-3, C5-6 and FDIA point mutants all exhibit greatly reduced NMJ expression (Fig. 2B), with very little MTG::GFP observed in synaptic boutons, and few puncta present on the surrounding muscle surface. Since these CBD mutant proteins are all highly abundant and copiously secreted in the salivary gland (Fig. 2A), these point mutations appear to disrupt MTG axonal transport and/or protein maintenance in a tissue-specific manner. Of these point mutant variants, C2-3 shows the highest levels of synaptic MTG::GFP expression (Fig. 2B), and so was chosen for examination in subsequent structure-function analyses. ΔCBD is used as the primary tool in all following studies, however, as it was the only mutant variant to show strong expression at the NMJ synapse.

MTG is secreted into the Subsynaptic Reticulum (SSR) domain and beyond

MTG is secreted from the motor neuron into the extracellular space between the synaptic terminal and muscle. We have previously used immuno-electron microscopy to show that MTG is present in the extracellular matrix adjacent to active zones, in the cleft

synaptomatrix (Rohrbough et al., 2007). However, in addition to the synaptomatrix, MTG::GFP is more widely distributed in the perisynaptic surrounding boutons (for example, see Fig. 1C), as we have reported previously (Rohrbough et al., 2007). To define MTG distribution at the NMJ more carefully, here we use the anti-Discs Large (DLG) marker, which labels the muscle subsynaptic reticulum (SSR), the extensive membrane folds surrounding type 1b synaptic boutons (Lahey et al., 1994). We have previously shown that loss of MTG alters distribution of several SSR proteins, including DLG (Rohrbough et al., 2007). The wandering 3rd instar NMJ expressing wildtype MTG::GFP driven only in the presynaptic terminal with *elav*-Gal4 was co-stained with anti-DLG (Fig. 4). In this case, it was necessary to use detergent to expose the DLG antigen to antibody, and as a consquence, both intracellular and extracellular MTG fluorescence were amplified with anti-GFP. As always, MTG is distributed in a collection of punctae within and surrounding synaptic boutons (Fig. 4). As expected, the majority of punctae are within the SSR domain defined by the presence of DLG (arrows in Fig. 4), while a minority of the punctae are found clearly beyond this domain (arrowheads in Fig. 4). Thus, MTG is found primarily within the DLG-defined synaptic domain of boutoun and surrounding SSR, but extends slightly beyond this domain.

The CBD restricts MTG synaptic extracellular diffusion

What role does the CBD play in MTG function? We have previously hypothesized that CBD binding to glycans in the synaptic cleft is necessary for MTG to organize the glycan-rich synaptomatrix (Rohrbough et al., 2007; Rushton et al., 2009; Rohrbough and Broadie, 2010). Conversely, another possibility is that the CBD binds glycans to anchor MTG within the synaptic ECM. In much the same way, Agrin is extracellularly anchored to synaptic ECM and ECM receptors at the vertebrate NMJ (Gesemann et al., 1996; Denzer et al., 1997; Gesemann et al., 1998). For example,Agrin binds to glycans present on α–dystroglycan in the postsynaptic domain of the muscle membrane (Xia and Martin, 2002). Detailed examination of secreted ΔCBD MTG::GFP distribution at the *Drosophila* NMJ in detergent-free conditions supports this latter hypothesis (Fig. 5). ΔCBD MTG::GFP is less abundant within the HRP-defined NMJ region, and clearly more widely distributed around the terminal than the wildtype protein, consistent with greater migration of extracellular ΔCBD puncta from presynaptic boutons (Fig. 5A). To quantify MTG::GFP distribution, we measured the distance of WT and ΔCBD MTG::GFP puncta from the presynaptic terminal membrane labeled with Cy5-anti-HRP, using FITC-anti-GFP to enhance MTG::GFP visualization. The distance between MTG::GFP puncta and nearest bouton membrane was measured for the 5 most distant puncta in each nerve terminal. The mean maximal puncta distance was 2.66 ± 0.28 μM (N=10 NMJs, 5 animals) for wildtype, compared to 4.09 ± 0.33 μM (N=10 NMJs, 5 animals) for ΔCBD NMJs, a highly significant >50% increase (P=0.003; Fig. 5C). C2-3 mutant MTG::GFP could not be analyzed in parallel since the puncta fluorescence is too dim for quantification. These results suggest that the CBD is required to bind/anchor MTG locally at the NMJ to mediate its synaptogenic function.

To test the functional consequence of CBD mutation, the ubiquitous UH1-GAL4 driver was used to express wildtype, ΔCBD and C2-3 point mutant MTG::GFP in the mtg^{1} null background to assay rescue of mutant phenotypes. Null *mtg* homozygotes are 100% embryonic lethal and totally paralyzed (Rohrbough et al., 2007). Transgenic expression of wildtype MTG::GFP fully rescues this phenotype, including embryonic movement and viability (Rushton et al., 2009; and this study). 100% of wildtype MTG::GFP rescued *mtg* null mutants are postembryonic viable, compared to the fully penetrant embryonic lethality of the null mutant, although most larvae and pupae still die during later development. By maturity, 20% of expected mtg^{1} null homozygotes are fully rescued to adult viability by UH1-GAL4 driven wildtype MTG::GFP, with fertile adult females. Unexpectedly, ΔCBD

MTG::GFP also rescues embryonic movement, although movement is weaker and only a small number of embryos hatch. However, all ΔCBD larvae die almost immediately, either partially within the egg-case, or after crawling an egg-length or two before arrest. Thus, ΔCBD MTG confers only very limited rescue of movement and viability compared to wildtype MTG. Similarly, the C2-3 point mutant variant rescues limited embryonic movement and hatching, and C2-3 larvae sometimes crawl a short distance. Importantly, however, like ΔCBD, C2-3 mutant larvae die shortly after hatching, and no ΔCBD or C2-3 mutant MTG::GFP expressing *mtg*^{1} null animals ever survive beyond the first instar. We conclude that the CBD of MTG clearly plays an essential function in sustaining postembryonic movement and viability.

The MTG CBD restricts glutamate receptor number at the synapse

Null *mtg*^{1} mutant embryos exhibit a profound defect in NMJ synaptogenesis, characterized by a failure to normally localize the postsynaptic proteins that drive glutamate receptor (GluR) domain assembly (Rohrbough et al., 2007). We previously showed that ubiquitous expression of wildtype MTG::GFP rescues GluR localization and functional defects in *mtg*^{1} null mutants (Rushton et al., 2009; Rohrbough and Broadie, 2010). We hypothesized that the CBD mutant variants would fail to rescue these synaptogenic defects. This hypothesis appeared well supported by the limited rescue of embryonic movement/viability by ΔCBD and C2-3 mutants, which would be consistent with weak/defective postsynaptic functional differentiation. To test this hypothesis, we assayed postsynaptic functional development using both imaging and electrophysiological tests at the mature embryonic (20–22 hrs AEL) NMJ in four genotypes; *mtg*^{1} null mutants and null mutants with UH1-GAL4 driven expression of wildtype, ΔCBD and C2-3 point mutant MTG::GFP (Fig. 6).

GluR expression and postsynaptic localization was first tested using an antibody against the essential GluRIIC subunit contained in all functionally assembled glutamate receptors (Fig. 6A) (Marrus et al., 2004). Null *mtg*^{1} NMJs exhibit severely reduced levels of postsynaptic GluR expression, while wildtype MTG::GFP rescued mutants display clear punctate GluR domains clustered at HRP-labeled NMJ boutons, indistinguishable from wildtype embryos (Fig. 6A; four ventral longitudinal muscles 7, 6, 13 and 12). Surprisingly, expression of both ΔCBD and C2-3 mutant MTG:GFP variants results in robustly concentrated synaptic GluR puncta (Fig. 6A, lower panels). Indeed, the intensity of GluR labeling in both CBD deletion and point mutant variants is clearly and consistently elevated compared to the wildtype MTG::GFP rescued condition. Postsynaptic anti-GluR mean fluorescence intensity and expression area was measured (Fig. 6B). The intensity for the *mtg*^{1} null was 33.8 ± 1.3 compared to *mtg*^{1} rescued with wildtype MTG::GFP of 117.0 ± 3.6, whereas *mtg*^{1} expressing the ΔCBD variant had an intensity of 144.0 ± 5.0 and C2–3 was 144.0 ± 7.1 (Fig. 6B, top). Thus, GluR abundance was significantly (P=0.005) increased in both ΔCBD and C2–3 mutant CBD expressing lines, compared to the wildtype rescue condition. The normalized area of synaptic GluR fluorescence was reduced to 43.4 ± 10.2% in *mtg*^{1} nulls, compared to *mtg*^{1} rescued with wildtype MTG::GFP (100 ± 9.8%). Although, GluR area was not significantly altered in *mtg*^{1} mutants expressing ΔCBD MTG (89 ± 4.5%), the C2–3 GluR area was significantly increased to 150 ± 8.9% (P=0.005; Fig. 6B, bottom). These results indicate, surprisingly, that the CBD is not required for GluR localization, but rather that CBD disruption elevates GluRs at the developing synapse, showing that MTG both facilitates and limits GluR recruitment to the postsynaptic domain during synaptogenesis.

To functionally test synaptic development, postsynaptic currents elicited by focally applied glutamate were recorded in whole-cell patch-clamp configuration from embryonic muscle 6 (Fig. 6A). Representative glutamate-gated current responses are shown for the five genotypes compared in Figure 6C. The *mtg*^{1} null mutant exhibits strongly reduced GluR currents compared to wildtype control, as well as to any of the CBD mutant variants

expressed in the null background (Fig. 6C). To quantify this observation, peak glutamate-gated current amplitudes were measured and compared between all five genotypes. The *mtg*^{1} mutant glutamate response was strongly reduced (45 ± 8% of wildtype control; $P<0.005$), and completely rescued by expression of wildtype MTG::GFP (116 ± 8% of control; Fig. 6D). Likewise, the ΔCBD and C2-3 mutant variants of MTG restored robust glutamate responses, displaying comparable rescue capabilities to wildtype MTG::GFP ($P\geq0.53$; Fig. 6D). These results indicate that although disruption of the CDB alters MTG localization at the synapse and fails to rescue movement and viability impairments, the CBD is not required for the functional differentiation of postsynaptic GluR domains.

MTG binds GlcNAc in a calcium-dependent manner

One possible explanation for the above findings is that the CBD does not perform the hypothesized function in glycan binding (Broadie et al., 2011; Dani and Broadie, 2011). Consistent with this possibility, the CBD does not appear to be required for binding of MTG near cell surfaces in the salivary gland and surrounding NMJs (Fig. 2A), although loss of the CBD does alter the extracellular distribution/anchoring of MTG surrounding the NMJ (Fig. 5). To explore this question, MTG binding to glycans was tested for wildtype MTG and for protein lacking the CBD. As a first step, the predicted MTG binding to GlcNAc was assayed on beads. MTG::GFP salivary gland lysates were incubated with carbohydrate-conjugated beads, compared to control lysates of salivary glands expressing GFP alone (Fig. 7A). The proteins were pulled down after bead incubation and analyzed by SDS-PAGE. Colloidal brilliant blue staining of total lysate reveals a large number of bands, as expected, but the bead fraction has very few protein bands by comparison (Fig. 7A, left). Duplicate samples on Western blots labeled for anti-GFP show MTG::GFP both in the lysate and the bead fractions, whereas GFP alone is found only in the lysate (Fig. 7A, right). Thus, as predicted, MTG::GFP demonstrates binding to GlcNAc.

Interestingly, this binding was discovered to be Ca^{2+}-dependent (Fig. 7B). To investigate the Ca^{2+}-dependence of binding, wildtype MTG::GFP lysate was prepared, divided into equivalent samples, and calcium was added in concentrations ranging from 0 – 5mM (0, 0.05, 0.1, 0.5, 1.0 and 5.0 mM) for incubation with GlcNAc beads (Fig. 7B). At Ca^{2+} concentrations <0.1 mM, there is reduced binding of MTG to GlcNAc beads (b); most of the MTG protein is present in the post-bead supernatant (s). At Ca^{2+} concentrations >0.1 mM, and especially at >1.0 mM, MTG binding to GlcNAc beads is substantially increased (Fig. 7B). At 5 mM Ca^{2+}, MTG protein in the supernatant is reduced to ≤50%, and MTG protein on the beads increased ≥160% compared to the 0.5 mM Ca^{2+} condition. In all cases, MTG binding to the beads was GlcNAc specific, as MTG could be eluted from the beads by free GlcNAc (0.4M) in the presence of elevated Ca^{2+} (Fig. 7B). Disconcertingly, however, MTG exhibited a broader than expected range of carbohydrate binding. Binding properties were assayed by incubating MTG::GFP and GFP control lysates with GlcNAc- conjugated agarose beads, compared to control unconjugated agarose beads, and to non-agarose chitin beads, in the presence and absence of elevated Ca^{2+} (Fig. 7C). Chitin, a polymer of GlcNAc, was expected to bind MTG, but agarose (galactose polymer) was not expected to bind. In the absence of Ca^{2+}, MTG::GFP was in the post-bead supernatant for all three bead types, whereas in the presence of elevated Ca^{2+}, most of the MTG::GFP was bound to all three classes of beads (Fig. 7C). In contrast, GFP alone showed no binding to any of the beads in the presence or absence of Ca^{2+} (shown for agarose beads). Thus, the carbohydrate-binding properties of MTG show that it is a lectin, and the Ca^{2+}-dependent nature of binding suggests it functions like a C-type lectin or neuronal pentraxin, such as Narp, which likewise bind in a Ca^{2+}-dependent manner (Tsui et al., 1996). Although MTG binds multiple glycans, free GlcNAc competes MTG from agarose-GlcNAc beads, indicating some GlcNAc specificity (Fig. 7B). To assay whether the CBD is required for this binding, ΔCBD

MTG::GFP lysate was incubated on GlcNAc beads in the presence and absence of elevated Ca^{2+} (Fig. 7D). Surprisingly, the ΔCBD protein variant still bound the GlcNAc beads in a Ca^{2+}-dependent manner (Fig. 7D). We conclude that the CBD does not mediate the lectin binding properties of MTG and that another cryptic carbohydrate-binding domain must be present.

MTG acts as a C-lectin to bind glycosylated proteins

MTG acting like a secreted Ca^{2+}-dependent lectin would be predicted to bind glycosylated proteins/proteoglycans in the extracellular space (Aspberg et al., 1995; Aspberg et al., 1997; O'Brien et al., 1999). To test for this predicted binding activity, we performed immunoprecipitation (IP) using anti-GFP-crosslinked Dynabeads on wildtype MTG::GFP, ΔCBD MTG::GFP, and GFP alone control tissue lysates (Fig. 8). As expected, MTG::GFP and GFP alone were both pulled down by anti-GFP IP (Fig. 8A, left). Duplicate samples were probed with the anti-HRP glycan probe, which recognizes a class of N-linked complex glycans known as the HRP-epitope glycans, characterized by α3- and α6-linked fucose moieties on the asparagine-linked GlcNAc in the glycan chain (Kurosaka et al., 1991; Wilson et al., 1998). These moieties are found almost exclusively on neuronal membrane proteins and pericellular ECM, which are very highly abundant at the NMJ synapse. For example, neuronal Fasciclins 1 and 2, Neurotactin and Nervana are HRP-modified, whereas non-neuronal forms are not (Jan and Jan, 1982; Snow et al., 1987; Desai et al., 1994). As expected, MTG::GFP lysates pull down a number of HRP-epitope glycans, whereas control GFP lysates pulled down no HRP-epitope glycans (Fig. 8A, right). In particular, MTG::GFP pulled down a major band of ~115 kDa and several minor bands between 60 and 115 kDa. In contrast, two key changes were observed for the ΔCBD lysate IP. First, surprisingly, the CBD protein pulled down more HRP-epitope glycans (Fig. 8A, right). Second, the most abundant band was ~94 kDa, while the 115 kDa band was greatly reduced (Fig. 8A, right). Thus, MTG binds HRP-epitope N-glycans, and the ΔCBD mutant variant MTG HRP-epitope glycan binding profile was very significantly altered, but not lost. Repeated proteomic analyses of the IP proteins have so far failed to identify the specific proteins altered.

Glycosylation plays an important role in the binding properties of lectins. We therefore assayed MTG glycosylation using O-deglycosidases and PNGaseF, both together and separately, to detect O- and N-linked glycosylation, respectively. None of the O-deglycosidases altered MTG size, but PNGaseF reduced MTG size by approx 4 kDa (data not shown). To address whether MTG is HRP-epitope modified, we carried out MTG::GFP pull-down experiments using GlcNAc beads, and then labeled with anti-HRP on Western blots. No MTG band (105 kDa) was observed (data not shown), showing that MTG itself is not HRP-modified. Lectins have been used to assay for glycans on Western blots, also known in this context as Far Western, Eastern or Far Eastern blots (Smalheiser and Kim, 1995; Ishikawa and Taki, 2000). Given MTG acts like a lectin, it should similarly bind to proteoglycans immobilized on a membrane. To test this prediction, the binding properties of MTG::GFP were assayed on protein samples from 1) developing embryos and 2) the adult nervous system. Tissue lysates were made from either late-stage embryos (16–22 hours AEL) or adult brains, with Western blots done using PVDF membranes (Fig. 8B). Membranes were labeled with fluorescent wheat germ agglutinin (WGA) lectin and glycan-binding anti-HRP. Both lectin labels revealed multiple bands, showing that glycosylated proteins were detectable. Similarly, the MTG::GFP lysate revealed multiple bands, whereas GFP alone recognized no detectable glycan bands (Fig. 8B). A number of bands appear to be common between the WGA, anti-HRP and MTG::GFP probes, indicating likely common glycan targets, although others were unique to MTG. These data clearly show that MTG is N-glycosylated and binds HRP-epitope proteins, but is not itself an HRP epitope protein. In

conclusion, we have shown that MTG binds to N-glycosylated proteins, but that the CBD is not required for this binding. The CBD does, however, strongly modulate this binding, both *in vitro* and *in vivo*, and acts to properly anchor MTG in the extracellular space surrounding NMJ synaptic boutons.

DISCUSSION

Our core hypothesis for the role of Mind-the-Gap (MTG) in synaptogenesis has proven to be wrong. We postulated that MTG is secreted from the presynaptic neuron to bind extracellular glycans via a well-conserved carbohydrate-binding domain, in order to build an extracellular synaptomatrix required for the anterograde *trans*-synaptic signaling inducing postsynaptic glutamate receptor (GluR) domains (Rohrbough et al., 2007; Rushton et al., 2009; Rohrbough and Broadie, 2010). Here, we undertook to systematically test this hypothesis with structure-function analyses of signal peptide (SP) and carbohydrate-binding domain (CBD) requirements *in vivo*. We confirmed that the SP is required for secretion and also discovered that MTG is strongly down-regulated when introduction into the secretory pathway is prevented. However, contrary to our hypothesis, the CBD is not required for binding glycans (as shown *in vitro* on GlcNAc-conjugated beads), glycoproteins (as shown by immunoprecipitation of HRP-epitope proteins), or binding to the extracellular membrane and/or pericellular matrix (as shown by *in vivo* imaging). The CBD does play an important regulatory role in the localization/anchoring of MTG in the synaptic ECM, since ΔCDB MTG migrates much further from the secretory synaptic boutons. This function may well be dependent on glycan binding, as indicated by the alteration in glycoprotein binding in ΔCDB MTG immunoprecipitation experiments. Moreover, contrary to our hypothesis, the CBD is not required for the MTG role in functional GluR postsynaptic localization during embryonic synaptogenesis. Rather, the CDB plays an unexpected role in limiting GluR recruitment to the developing NMJ synapse, and is essential for postembryonic viability.

Although the CDB requirement is clearly fundamentally different from our previous hypothesis, this structure-function analysis reveals intriguing CDB functions. The MTG CBD has a strong homology to CBD14 (Rohrbough et al., 2007), yet it is not required for binding to GlcNAc, GlcNAc polymer or other glycans, showing that another cryptic CDB must be present which is sufficient to mediate this carbohydrate binding. Candidate carbohydrate-binding regions include the glutamine-rich region near the N-terminus, and the coiled-coil domain near the C terminus (Fig. 1A). The glutamine-rich region is a particularly intriguing candidate. This domain bears a striking resemblance to the prion-like domains of *Aplysia* CPEB (Si et al. 2010) and *Drosophila* CPEB (Orb2) (Keleman et al., 2007), as well as *Drosophila* Fragile X Mental Retardation Protein (FMRP) (Banerjee et al., 2010), all of which are necessary for synaptic mechanisms underlying learning and memory. Interestingly, the prion-like domain of *Aplysia* CPEB causes mouse CPEB (which lacks this domain) to aggregate into puncta, very similar to MTG puncta (Si et al. 2010). Similarly, the FMRP prion-like domain drives aggregation and puncta formation (Banerjee et al., 2010). It would therefore be of great interest to extend our structure-function analysis to the MTG glutamine-rich region, specifically to investigate whether this domain is involved in carbohydrate-binding and/or extracellular puncta formation.

Endogenous animal lectins are extremely diverse, and are organized into many families, including C-type, R-type, siglecs, galectins and chitinase-like lectins (Shen and Jacobs-Lorena, 1999; Dodd and Drickamer, 2001; Zaheer ul et al., 2007), among others. Each lectin family has characteristic carbohydrate-binding-fold consensus sequences, which differ greatly from one family to another. Within several families, examples exist of lectins that have the characteristic disulfide-bonding fold domain, but nevertheless do not bind predicted carbohydrate substrates. For example, the C-lectin family includes several members with

canonical C-type Lectin Domains (CTLD) that do not bind carbohydrates, nor is calcium always required for their carbohydrate binding (Drickamer and Dodd, 1999; Dodd and Drickamer, 2001). Specifically, collectin-like tetranectin binds calcium and the protein kringle 4 via its CTLD, yet binds the carbohydrate heparin in a separate, non-CTLD domain (Lorentsen et al., 2000). Likewise, while lecticans bind tenascin-R in a Ca^{2+}-dependent manner, this binding does not require tenascin-linked carbohydrates, but rather appears to be a protein-protein interaction (Aspberg et al., 1997). Thus, the relationship between lectins and their carbohydrate binding partners is not simple nor easily defined, and it is obvious that CBDs acquire new functions and new binding properties during evolution. This certainly appears to be the case for the MTG CBD, which is not required for carbohydrate binding yet regulates MTG mobility/anchoring at the NMJ, and regulates the recruitment of postsynaptic GluRs.

It is particularly intriguing that MTG carbohydrate binding is Ca^{2+}-dependent, and it is tempting to place MTG in the C-type lectin family based on this characteristic. However, MTG lacks a canonical CTLD (Zelensky and Gready, 2005), and does not appear to resemble any of the very diverse but well-characterized C-type lectin families (Dodd and Drickamer, 2001; Zelensky and Gready, 2005). Nor does it resemble the pentraxin domain, another Ca^{2+}-dependent lectin domain. Rather, MTG has the CBD14 domain of the peritrophin lectin family (Shen and Jacobs-Lorena, 1999; Rohrbough et al., 2007). Invertebrate lectins of this family have not been reported to require calcium for carbohydrate binding, although the related *Clostridium* endo beta-1.3-glucanase Lic16A binds GlcNAc polymer far more strongly in the presence of calcium (Dvortsov et al., 2009) and the related mammalian FIBCD1 also has a Ca^{2+}-dependent binding requirement (Schlosser et al., 2009). We speculate that the calcium requirement for MTG binding to synaptic carbohydrates may be physiologically important, since extracellular calcium concentration in the synaptic cleft and surrounding synaptomatrix is modulated by synaptic activity, involving pre-and postsynaptic calcium influx and calcium exchange (Sheng and Kim, 2002; Frank et al., 2006; Zhao et al., 2011).

Although the MTG CDB has homology to chitin-binding domains, there is no indication that MTG binds chitin *in vivo*. MTG does not localize in chitin-rich tissues, and when exogenously expressed in these tissues is not retained to any detectable degree. When MTG::GFP is expressed ubiquitously, the protein does not localize in the trachea, nor in other chitinous structures such as the external cuticle. In contrast, *Drosophila* Serp and Verm chitin deacetylases with canonical chitin-binding domains strongly co-localize with chitin in the trachea, and a Serp N-terminus construct with the SP and CBD fused to GFP likewise strongly co-localizes with chitin in the trachea (Luschnig et al., 2006). Indeed, it is very striking that MTG is strongly downregulated outside nervous tissue when driven ubiquitously, and does not detectably accumulate in epidermis or muscle, except immediately surrounding the NMJ terminal. Thus, there must be a mechanism to specifically retain and preserve MTG in neurons, particularly in synaptic domains. Likewise, within the embryonic CNS, expression of MTG is virtually identical whether it is driven by a neural-specific or a ubiquitous GAL4 driver (Rushton et al., 2009), indicating that MTG::GFP is accumulated at synapses in a very specific manner and downregulated elsewhere. The one notable exception is the salivary gland, a tissue specialized for secretion, but it appears even the salivary gland cannot maintain MTG without the SP required for secretion into the extracellular lumenal domain. These data suggest that MTG likely binds GlcNAc inside the chains of N-glycans, O-glycans and/or glycosaminoglycans (GAGs) within the pericellular matrix and particularly within the specialized extracellular synaptomatrix.

How might the MTG CBD affect synaptic functional development? It is well established that ECM glycoproteins and proteoglycans are essential for the organization of synaptic

components (see recent review by (Dani and Broadie, 2011)). Lectins that bind selectively to the carbohydrate component of these molecules can regulate, modulate, stabilize or sequester their activities (see recent review by (Dansie and Ethell, 2011)). At the vertebrate NMJ, the Agrin lectin is required for AChR cluster maintenance in a fashion similar to the MTG requirement for GluR localization at the *Drosophila* NMJ (Rupp et al., 1991; Tsim et al., 1992, McDonnell, 2004 #17, Rohrbough, 2007 #1; Tsen et al., 1995). In the vertebrate CNS, lecticans brevican and neurocan bind to tenascin and hyaluronic acid to stabilize the extracellular synaptomatrix lattice, and have been implicated in affecting synaptic development and plasticity (Zhou et al., 2001; Brakebusch et al., 2002). Digestion of this lattice by hyaluronidase causes increased lateral diffusion of AMPA GluRs (Frischknecht et al., 2009), suggesting the matrix acts as an important diffusion/mobility barrier. Similarly, the neuronal pentraxin (NP) lectin family has been implicated in AMPA GluR trafficking: NP-1 and NP-2 (also known as Narp) form a complex with the NP receptor to colocalize with and trigger clustering of AMPA GluRs at postsynaptic sites (O'Brien et al., 1999; O'Brien et al., 2002; Xu et al., 2003; Sia et al., 2007; Cho et al., 2008). Specifically, this lectin mechanism mediates postsynaptic recruitment of the AMPA GluRs with GluR1 and GluR4 subunits (reviewed in (Dansie and Ethell, 2011)). Our results in the current study show that the CBD of MTG is similarly important for regulating GluR trafficking and postsynaptic maintenance at the *Drosophila* developing embryonic NMJ.

In conclusion, we have shown that MTG is a secreted, Ca^{2+}-dependent carbohydrate-binding protein resident in the extracellular matrix surrounding synapses. The predicted signal peptide is required for the secretion of MTG, but the carbohydrate-binding domain is not demonstrably required for glycan interaction, indicating that a cryptic carbohydrate-binding domain must also be present within MTG. The CBD appears to regulate binding affinity of MTG to the ECM, and is clearly required to properly anchor MTG close to the synaptic interface. In the absence of the CBD, excess GluRs are recruited to the embryonic NMJ postsynaptic domain. This is the opposite consequence to the loss of postsynaptic GluRs occurring with complete removal of MTG. We conclude that the MTG lectin has both positive and negative roles regulating GluR recruitment during synaptogenesis.

Acknowledgments

We thank Aaron DiAntonio for his generous gift of the GluRIIC antibody. We thank Qing-Xia Chen for her excellent technical assistance. This work was supported by National Institutes of Health RO1 grant GM54544 to K.B.

References

Arakane Y, Zhu Q, Matsumiya M, Muthukrishnan S, Kramer KJ. Properties of catalytic, linker and chitin-binding domains of insect chitinase. Insect Biochem Mol Biol. 2003; 33:631–648. [PubMed: 12770581]

Aspberg A, Binkert C, Ruoslahti E. The versican C-type lectin domain recognizes the adhesion protein tenascin-R. Proc Natl Acad Sci U S A. 1995; 92:10590–10594. [PubMed: 7479846]

Aspberg A, Miura R, Bourdoulous S, Shimonaka M, Heinegard D, Schachner M, Ruoslahti E, Yamaguchi Y. The C-type lectin domains of lecticans, a family of aggregating chondroitin sulfate proteoglycans, bind tenascin-R by protein-protein interactions independent of carbohydrate moiety. Proc Natl Acad Sci U S A. 1997; 94:10116–10121. [PubMed: 9294172]

Banerjee P, Schoenfeld BP, Bell AJ, Choi CH, Bradley MP, Hinchey P, Kollaros M, Park JH, McBride SM, Dockendorff TC. Short- and long-term memory are modulated by multiple isoforms of the fragile X mental retardation protein. J Neurosci. 2010; 30:6782–6792. [PubMed: 20463240]

Brakebusch C, Seidenbecher CI, Asztely F, Rauch U, Matthies H, Meyer H, Krug M, Bockers TM, Zhou X, Kreutz MR, Montag D, Gundelfinger ED, Fassler R. Brevican-deficient mice display

impaired hippocampal CA1 long-term potentiation but show no obvious deficits in learning and memory. Mol Cell Biol. 2002; 22:7417–7427. [PubMed: 12370289]

Broadie K, Baumgartner S, Prokop A. Extracellular matrix and its receptors in Drosophila neural development. Dev Neurobiol. 2011

Cho RW, Park JM, Wolff SB, Xu D, Hopf C, Kim JA, Reddy RC, Petralia RS, Perin MS, Linden DJ, Worley PF. mGluR1/5-dependent long-term depression requires the regulated ectodomain cleavage of neuronal pentraxin NPR by TACE. Neuron. 2008; 57:858–871. [PubMed: 18367087]

Dani N, Broadie K. Glycosylated synaptomatrix regulation of trans-synaptic signaling. Dev Neurobiol. 2011

Dansie LE, Ethell IM. Casting a net on dendritic spines: The extracellular matrix and its receptors. Dev Neurobiol. 2011; 71:956–981. [PubMed: 21834084]

Denzer AJ, Brandenberger R, Gesemann M, Chiquet M, Ruegg MA. Agrin binds to the nerve-muscle basal lamina via laminin. J Cell Biol. 1997; 137:671–683. [PubMed: 9151673]

Desai CJ, Popova E, Zinn K. A Drosophila receptor tyrosine phosphatase expressed in the embryonic CNS and larval optic lobes is a member of the set of proteins bearing the “HRP” carbohydrate epitope. J Neurosci. 1994; 14:7272–7283. [PubMed: 7527841]

Dodd RB, Drickamer K. Lectin-like proteins in model organisms: implications for evolution of carbohydrate-binding activity. Glycobiology. 2001; 11:71R–79R.

Drickamer K, Dodd RB. C-Type lectin-like domains in Caenorhabditis elegans: predictions from the complete genome sequence. Glycobiology. 1999; 9:1357–1369. [PubMed: 10561461]

Dvortsov IA, Lunina NA, Chekanovskaya LA, Schwarz WH, Zverlov VV, Velikodvorskaya GA. Carbohydrate-binding properties of a separately folding protein module from beta-1,3-glucanase Lic16A of Clostridium thermocellum. Microbiology. 2009; 155:2442–2449. [PubMed: 19389758]

Fabian RH, Coulter JD. Transneuronal transport of lectins. Brain Res. 1985; 344:41–48. [PubMed: 2412649]

Featherstone DE, Chen K, Broadie K. Harvesting and preparing Drosophila embryos for electrophysiological recording and other procedures. J Vis Exp. 2009

Frank CA, Kennedy MJ, Goold CP, Marek KW, Davis GW. Mechanisms underlying the rapid induction and sustained expression of synaptic homeostasis. Neuron. 2006; 52:663–677. [PubMed: 17114050]

Frischknecht R, Heine M, Perrais D, Seidenbecher CI, Choquet D, Gundelfinger ED. Brain extracellular matrix affects AMPA receptor lateral mobility and short-term synaptic plasticity. Nat Neurosci. 2009; 12:897–904. [PubMed: 19483686]

Gesemann M, Brancaccio A, Schumacher B, Ruegg MA. Agrin is a high-affinity binding protein of dystroglycan in non-muscle tissue. J Biol Chem. 1998; 273:600–605. [PubMed: 9417121]

Gesemann M, Cavalli V, Denzer AJ, Brancaccio A, Schumacher B, Ruegg MA. Alternative splicing of agrin alters its binding to heparin, dystroglycan, and the putative agrin receptor. Neuron. 1996; 16:755–767. [PubMed: 8607994]

Gonatas NK, Harper C, Mizutani T, Gonatas JO. Superior sensitivity of conjugates of horseradish peroxidase with wheat germ agglutinin for studies of retrograde axonal transport. J Histochem Cytochem. 1979; 27:728–734. [PubMed: 90065]

Hagihara K, Miura R, Kosaki R, Berglund E, Ranscht B, Yamaguchi Y. Immunohistochemical evidence for the brevican-tenascin-R interaction: colocalization in perineuronal nets suggests a physiological role for the interaction in the adult rat brain. J Comp Neurol. 1999; 410:256–264. [PubMed: 10414531]

Iglesias M, Ribera J, Esquerda JE. Treatment with digestive agents reveals several glycoconjugates specifically associated with rat neuromuscular junction. Histochemistry. 1992; 97:125–131. [PubMed: 1559843]

Ishikawa D, Taki T. Thin-layer chromatography blotting using polyvinylidene difluoride membrane (far-eastern blotting) and its applications. Methods Enzymol. 2000; 312:145–157. [PubMed: 11070868]

Itaya SK, van Hoesen GW. WGA-HRP as a transneuronal marker in the visual pathways of monkey and rat. Brain Res. 1982; 236:199–204. [PubMed: 6175378]

Jan LY, Jan YN. Antibodies to horseradish peroxidase as specific neuronal markers in Drosophila and in grasshopper embryos. Proc Natl Acad Sci U S A. 1982; 79:2700–2704. [PubMed: 6806816]

Kawabata S, Nagayama R, Hirata M, Shigenaga T, Agarwala KL, Saito T, Cho J, Nakajima H, Takagi T, Iwanaga S. Tachycitin, a small granular component in horseshoe crab hemocytes, is an antimicrobial protein with chitin-binding activity. J Biochem. 1996; 120:1253–1260. [PubMed: 9010778]

Keleman K, Kruttner S, Alenius M, Dickson BJ. Function of the Drosophila CPEB protein Orb2 in long-term courtship memory. Nat Neurosci. 2007; 10:1587–1593. [PubMed: 17965711]

Kurosaka A, Yano A, Itoh N, Kuroda Y, Nakagawa T, Kawasaki T. The structure of a neural specific carbohydrate epitope of horseradish peroxidase recognized by anti-horseradish peroxidase antiserum. J Biol Chem. 1991; 266:4168–4172. [PubMed: 1705547]

Lahey T, Gorczyca M, Jia XX, Budnik V. The Drosophila tumor suppressor gene dlg is required for normal synaptic bouton structure. Neuron. 1994; 13:823–835. [PubMed: 7946331]

Lin DM, Goodman CS. Ectopic and increased expression of Fasciclin II alters motoneuron growth cone guidance. Neuron. 1994; 13:507–523. [PubMed: 7917288]

Lorentsen RH, Graversen JH, Caterer NR, Thogersen HC, Etzerodt M. The heparin-binding site in tetranectin is located in the N-terminal region and binding does not involve the carbohydrate recognition domain. Biochem J. 2000; 347(Pt 1):83–87. [PubMed: 10727405]

Luschnig S, Batz T, Armbruster K, Krasnow MA. serpentine and vermiform encode matrix proteins with chitin binding and deacetylation domains that limit tracheal tube length in Drosophila. Curr Biol. 2006; 16:186–194. [PubMed: 16431371]

Marrus SB, Portman SL, Allen MJ, Moffat KG, DiAntonio A. Differential localization of glutamate receptor subunits at the Drosophila neuromuscular junction. J Neurosci. 2004; 24:1406–1415. [PubMed: 14960613]

Martin PT, Sanes JR. Role for a synapse-specific carbohydrate in agrin-induced clustering of acetylcholine receptors. Neuron. 1995; 14:743–754. [PubMed: 7718237]

McDonnell KM, Grow WA. Reduced glycosaminoglycan sulfation diminishes the agrin signal transduction pathway. Dev Neurosci. 2004; 26:1–10. [PubMed: 15509893]

O'Brien R, Xu D, Mi R, Tang X, Hopf C, Worley P. Synaptically targeted narp plays an essential role in the aggregation of AMPA receptors at excitatory synapses in cultured spinal neurons. J Neurosci. 2002; 22:4487–4498. [PubMed: 12040056]

O'Brien RJ, Xu D, Petralia RS, Steward O, Huganir RL, Worley P. Synaptic clustering of AMPA receptors by the extracellular immediate-early gene product Narp. Neuron. 1999; 23:309–323. [PubMed: 10399937]

Parkhomovskiy N, Kammesheidt A, Martin PT. N-acetyllactosamine and the CT carbohydrate antigen mediate agrin-dependent activation of MuSK and acetylcholine receptor clustering in skeletal muscle. Mol Cell Neurosci. 2000; 15:380–397. [PubMed: 10845774]

Parnas D, Haghighi AP, Fetter RD, Kim SW, Goodman CS. Regulation of postsynaptic structure and protein localization by the Rho-type guanine nucleotide exchange factor dPix. Neuron. 2001; 32:415–424. [PubMed: 11709153]

Ribera J, Esquerda JE, Comella JX. Phylogenetic polymorphism on lectin binding to junctional and non-junctional basal lamina at the vertebrate neuromuscular junction. Histochemistry. 1987; 87:301–307. [PubMed: 3121544]

Rohrbough J, Broadie K. Anterograde Jelly belly ligand to Alk receptor signaling at developing synapses is regulated by Mind the gap. Development. 2010; 137:3523–3533. [PubMed: 20876658]

Rohrbough J, Rushton E, Palanker L, Woodruff E, Matthies HJ, Acharya U, Acharya JK, Broadie K. Ceramidase regulates synaptic vesicle exocytosis and trafficking. J Neurosci. 2004; 24:7789–7803. [PubMed: 15356190]

Rohrbough J, Rushton E, Woodruff E 3rd, Fergestad T, Vigneswaran K, Broadie K. Presynaptic establishment of the synaptic cleft extracellular matrix is required for post-synaptic differentiation. Genes Dev. 2007; 21:2607–2628. [PubMed: 17901219]

Rupp F, Payan DG, Magill-Solc C, Cowan DM, Scheller RH. Structure and expression of a rat agrin. Neuron. 1991; 6:811–823. [PubMed: 1851019]

Rushton E, Rohrbough J, Broadie K. Presynaptic secretion of mind-the-gap organizes the synaptic extracellular matrix-integrin interface and postsynaptic environments. Dev Dyn. 2009; 238:554–571. [PubMed: 19235718]

Sanes JR, Cheney JM. Lectin binding reveals a synapse-specific carbohydrate in skeletal muscle. Nature. 1982; 300:646–647. [PubMed: 7144916]

Sarkar M, Iliadi KG, Leventis PA, Schachter H, Boulianne GL. Neuronal expression of Mgat1 rescues the shortened life span of Drosophila Mgat11 null mutants and increases life span. Proc Natl Acad Sci U S A. 2010; 107:9677–9682. [PubMed: 20457894]

Sarkar M, Leventis PA, Silvescu CI, Reinhold VN, Schachter H, Boulianne GL. Null mutations in Drosophila N-acetylglucosaminyltransferase I produce defects in locomotion and a reduced life span. J Biol Chem. 2006; 281:12776–12785. [PubMed: 16522637]

Schlosser A, Thomsen T, Moeller JB, Nielsen O, Tornoe I, Mollenhauer J, Moestrup SK, Holmskov U. Characterization of FIBCD1 as an acetyl group-binding receptor that binds chitin. J Immunol. 2009; 183:3800–3809. [PubMed: 19710473]

Scott LJ, Bacou F, Sanes JR. A synapse-specific carbohydrate at the neuromuscular junction: association with both acetylcholinesterase and a glycolipid. J Neurosci. 1988; 8:932–944. [PubMed: 3346730]

Shen Z, Jacobs-Lorena M. Evolution of chitin-binding proteins in invertebrates. J Mol Evol. 1999; 48:341–347. [PubMed: 10093224]

Sheng M, Kim MJ. Postsynaptic signaling and plasticity mechanisms. Science. 2002; 298:776–780. [PubMed: 12399578]

Si K, Choi YB, White-Grindley E, Majumdar A, Kandel ER. Aplysia CPEB can form prion-like multimers in sensory neurons that contribute to long-term facilitation. Cell. 2010; 140:421–435. [PubMed: 20144764]

Sia GM, Beique JC, Rumbaugh G, Cho R, Worley PF, Huganir RL. Interaction of the N-terminal domain of the AMPA receptor GluR4 subunit with the neuronal pentraxin NP1 mediates GluR4 synaptic recruitment. Neuron. 2007; 55:87–102. [PubMed: 17610819]

Smalheiser NR, Kim E. Purification of cranin, a laminin binding membrane protein. Identity with dystroglycan and reassessment of its carbohydrate moieties. J Biol Chem. 1995; 270:15425–15433. [PubMed: 7797531]

Snow PM, Patel NH, Harrelson AL, Goodman CS. Neural-specific carbohydrate moiety shared by many surface glycoproteins in Drosophila and grasshopper embryos. J Neurosci. 1987; 7:4137–4144. [PubMed: 3320283]

Tsen G, Halfter W, Kroger S, Cole GJ. Agrin is a heparan sulfate proteoglycan. J Biol Chem. 1995; 270:3392–3399. [PubMed: 7852425]

Tsim KW, Ruegg MA, Escher G, Kroger S, McMahan UJ. cDNA that encodes active agrin. Neuron. 1992; 8:677–689. [PubMed: 1314620]

Tsui CC, Copeland NG, Gilbert DJ, Jenkins NA, Barnes C, Worley PF. Narp, a novel member of the pentraxin family, promotes neurite outgrowth and is dynamically regulated by neuronal activity. J Neurosci. 1996; 16:2463–2478. [PubMed: 8786423]

Wairkar YP, Fradkin LG, Noordermeer JN, DiAntonio A. Synaptic defects in a Drosophila model of congenital muscular dystrophy. J Neurosci. 2008; 28:3781–3789. [PubMed: 18385336]

Wilson IB, Harthill JE, Mullin NP, Ashford DA, Altmann F. Core alpha1,3-fucose is a key part of the epitope recognized by antibodies reacting against plant N-linked oligosaccharides and is present in a wide variety of plant extracts. Glycobiology. 1998; 8:651–661. [PubMed: 9621106]

Xia B, Martin PT. Modulation of agrin binding and activity by the CT and related carbohydrate antigens. Mol Cell Neurosci. 2002; 19:539–551. [PubMed: 11988021]

Xiang YY, Dong H, Wan Y, Li J, Yee A, Yang BB, Lu WY. Versican G3 domain regulates neurite growth and synaptic transmission of hippocampal neurons by activation of epidermal growth factor receptor. J Biol Chem. 2006; 281:19358–19368. [PubMed: 16648628]

Xu D, Hopf C, Reddy R, Cho RW, Guo L, Lanahan A, Petralia RS, Wenthold RJ, O'Brien RJ, Worley P. Narp and NP1 form heterocomplexes that function in developmental and activity-dependent synaptic plasticity. Neuron. 2003; 39:513–528. [PubMed: 12895424]

Yamagata M, Sanes JR. Versican in the developing brain: lamina-specific expression in interneuronal subsets and role in presynaptic maturation. J Neurosci. 2005; 25:8457–8467. [PubMed: 16162928]

Zaheer ul H, Dalal P, Aronson NN Jr, Madura JD. Family 18 chitolectins: comparison of MGP40 and HUMGP39. Biochem Biophys Res Commun. 2007; 359:221–226. [PubMed: 17543889]

Zelensky AN, Gready JE. The C-type lectin-like domain superfamily. Febs J. 2005; 272:6179–6217. [PubMed: 16336259]

Zhao C, Dreosti E, Lagnado L. Homeostatic synaptic plasticity through changes in presynaptic calcium influx. J Neurosci. 2011; 31:7492–7496. [PubMed: 21593333]

Zhou XH, Brakebusch C, Matthies H, Oohashi T, Hirsch E, Moser M, Krug M, Seidenbecher CI, Boeckers TM, Rauch U, Buettner R, Gundelfinger ED, Fassler R. Neurocan is dispensable for brain development. Mol Cell Biol. 2001; 21:5970–5978. [PubMed: 11486035]

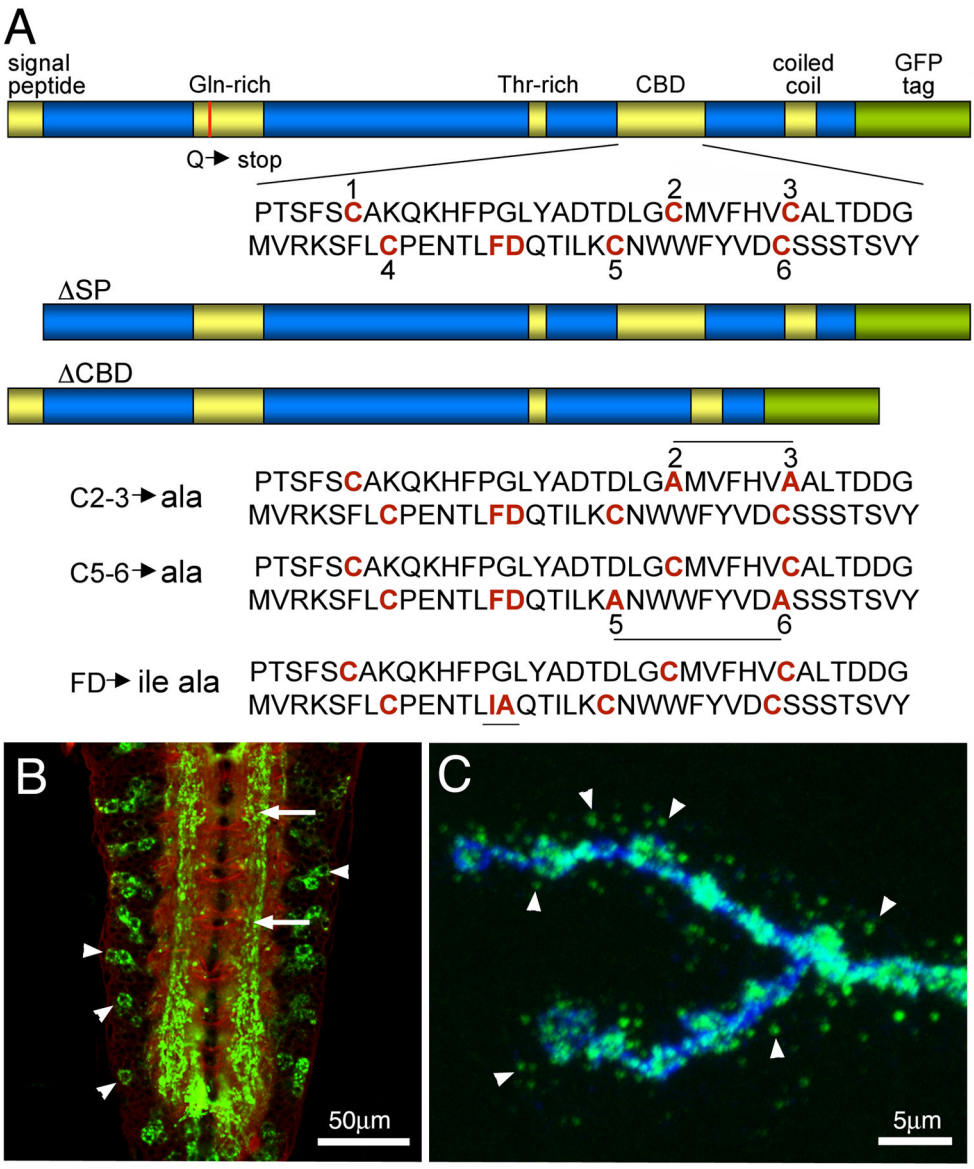

Fig 1. Transgenic constructs of the Mind-the-Gap (MTG) gene product

(A) Diagram of MTG protein domains in wildtype and transgenic mutant variants. The Signal Peptide (SP) is deleted in the ΔSP mutant and Carbohydrate Binding Domain (CBD) deleted in the ΔCBD mutant. The red line in the Gln-rich domain indicates the Q to stop point mutation in the *mtg*^{1} null. Shown below are the three point mutant variants in the CBD domain: conserved Cys (C) residues and Phe-Asp (F–D) residues are mutated in C2-3, C5-6, and FDIA transgenic lines, respectively. **(B)** Representative image of *elav*-driven MTG::GFP expression in the wandering 3rd instar ventral nerve cord, co-labeled with anti-HRP (red) and anti-GFP (green). Arrows point to MTG::GFP within the synaptic neuropil. Arrowheads point to MTG::GFP within neuronal somata. **(C)** Representative image of *elav*-driven MTG::GFP in the wandering 3rd instar neuromuscular junction (NMJ), co-labeled with anti-HRP (blue) and anti-GFP (green). The probes were applied in the absence of detergent, to highlight labeling of extracellular proteins. Arrowheads point to MTG::GFP secreted from the presynaptic motor neuron terminal, to form extracellular puncta surrounding NMJ synaptic boutons.

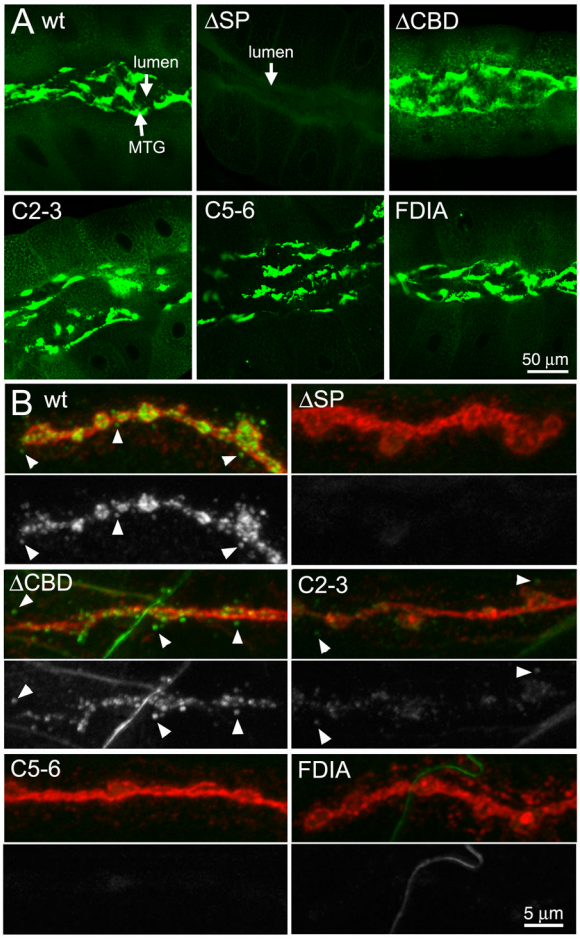

Fig 2. Expression of MTG mutant variants in the salivary gland and NMJ

Representative images of *elav*-driven transgenic wildtype (wt) and mutant MTG::GFP variants in wandering 3rd instar salivary gland (A, top 6 panels), and neuromuscular junction (B, bottom panels). **(A)** MTG::GFP detected in the salivary gland based on native GFP fluorescence, showing protein secretion into, and accumulation within, the extracellular lumen. **(B)** MTG::GFP detected at the NMJ based on anti-GFP (green), with neuronal membranes co-labeled with anti-HRP (red). NMJs were labeled without detergent to highlight detection of secreted extracellular MTG::GFP. For each MTG variant, the lower panel shows GFP alone, in white. Arrowheads show secreted MTG::GFP puncta surrounding NMJ synaptic boutons.

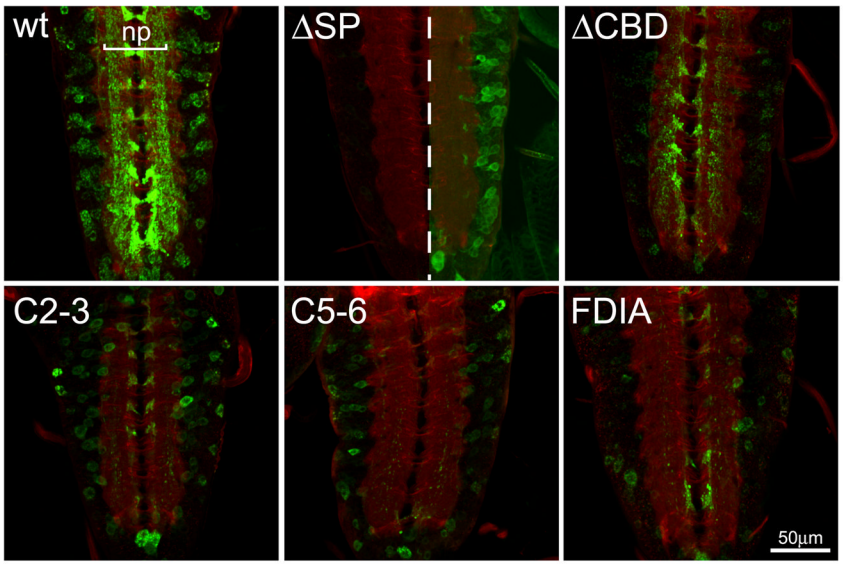

Fig 3. Expression of MTG mutant variants in the central nervous system

Representative images of *elav*-driven transgenic wildtype (wt) and mutant MTG::GFP variants in the CNS of wandering 3rd instar larvae. The CNS is labeled in the presence of detergent to permeabilize the tissue, co-labeled with anti-GFP (green) and anti-HRP (red) to mark neuronal membranes. In the wt control panel, the synaptic neuropil (np) is indicated. In the ΔSP panel, the central midline dotted line divides same gain as all other genotypes (left) and increased gain to show presence of neuronal soma expression of MTG::GFP (right).

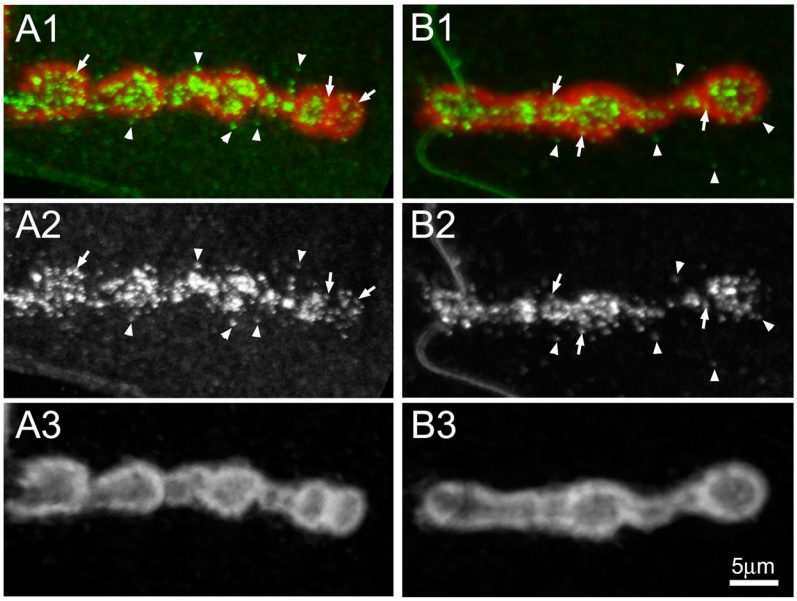

Fig 4. MTG is secreted into and beyond the subsynaptic reticulum domain

Representative images of wandering 3rd instar NMJ synapses expressing wildtype MTG::GFP (anti-GFP, green), co-labeled with anti-Discs Large (DLG, red) to reveal the muscle subsynaptic reticulum (SSR) surrounding NMJ boutons. Detergent was used to permeabilize cells, as DLG is an intracellular, membrane-associated scaffold protein. **(A1** and **B1)** Two example NMJ terminals showing co-labeling for MTG (green) and DLG (red) surrounding a series of adjacent synaptic boutons. **(A2** and **B2)** Same two NMJs, showing MTG fluorescence only in white. **(A3** and **B3)** Same two NMJs, showing DLG fluorescence only in white. Arrows indicate MTG puncta within the SSR domain defined by DLG. Arrowheads indicate MTG outside the SSR domain.

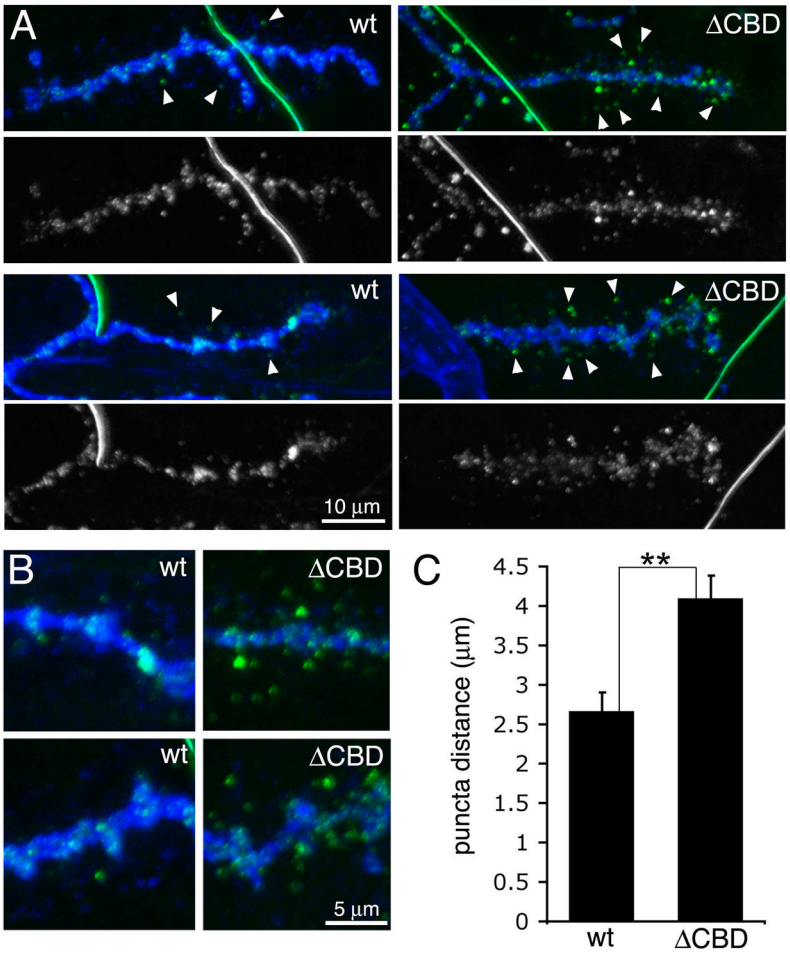

Fig 5. Deletion of CBD domain increases secreted MTG migration at the synapse

(A) Wandering 3rd instar NMJ synapses expressing wildtype (wt) MTG::GFP (left) or CBD MTG::GFP (right) driven by neuronal *elav*-GAL4, colabeled with anti-HRP (blue) and anti-GFP (green). Labeling was done without detergent, so that only extracellular proteins are enhanced. Arrowheads show secreted MTG::GFP puncta at a distance from the presynaptic terminal. **(B)** Higher magnification images showing increased migration from the presynaptic terminal of extracellular ΔCBD MTG::GFP compared with wildtype MTG::GFP. **(C)** Quantification of mean maximal distance of MTG::GFP puncta from the nearest neuronal membrane. Significance indicated (**) is P=0.003 using Wilcoxon rank sum test and Kruskal-Wallis test.

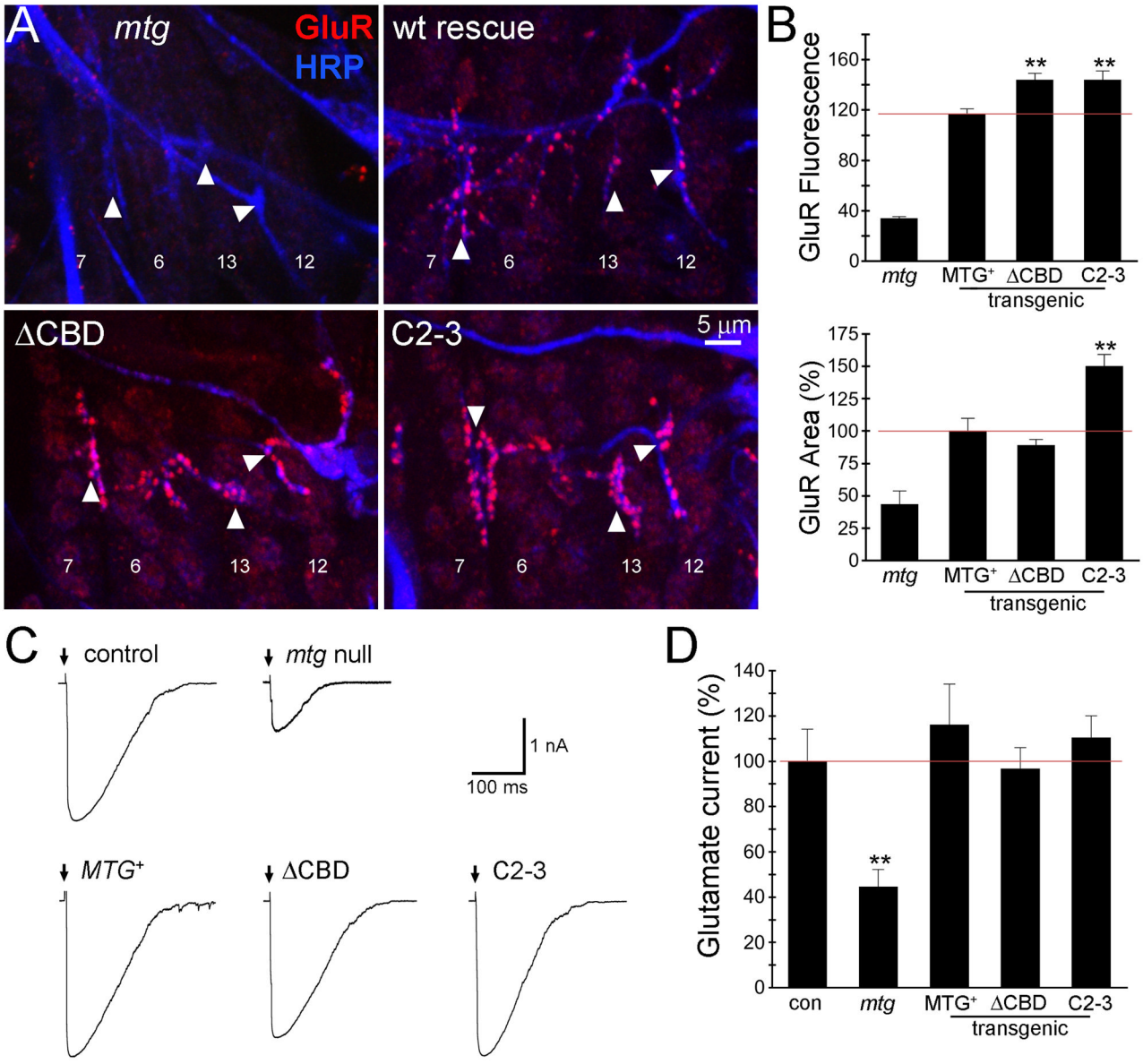

Fig 6. Mutation of CBD increases glutamate receptor abundance but not function

(A) Embryonic NMJs (20–22 hours after fertilization) in *mtg* null and transgenic MTG::GFP genotypes, co-labeled for anti-HRP (blue) and anti-glutamate receptor C subunit (GluR; red). Arrowheads indicate NMJs on ventral muscles 6, 7, 12 and 13 used for quantification. **(B)** Quantified postsynaptic GluR fluorescence intensity (top) and area (bottom; normalized to wildtype MTG::GFP rescue) in the four indicated genotypes. The red line indicates the value of wildtype MTG::GFP rescue of the mtg^1 null mutant phenotype. Asterisks indicate statistical significance (using one-way ANOVA) compared to the wildtype rescue condition (**P<0.005). Sample size is N = 5–6 hemisegments (15–18 NMJs) for each transgenic rescued genotype. **(C)** Representative postsynaptic currents elicited by iontophoretic glutamate application at embryonic NMJs in control (w^{1118}; UH1-GAL4/+), mtg^1 null mutant and the null mutant expressing wildtype MTG::GFP (MTG^+), ΔCBD deleted MTG:GFP and C2-3 point mutant MTG::GFP transgenic conditions. Glutamate was applied as indicated (arrows) to the NMJ 6 postsynaptic domain and currents recorded in the

voltage-clamped (−60 mV) muscle. **(D)** Quantified mean normalized glutamate response for all five genotypes. Asterisks indicate significance level compared to control (**P <0.005). Sample size is N = 7–10 embryos per each of the five genotypes.

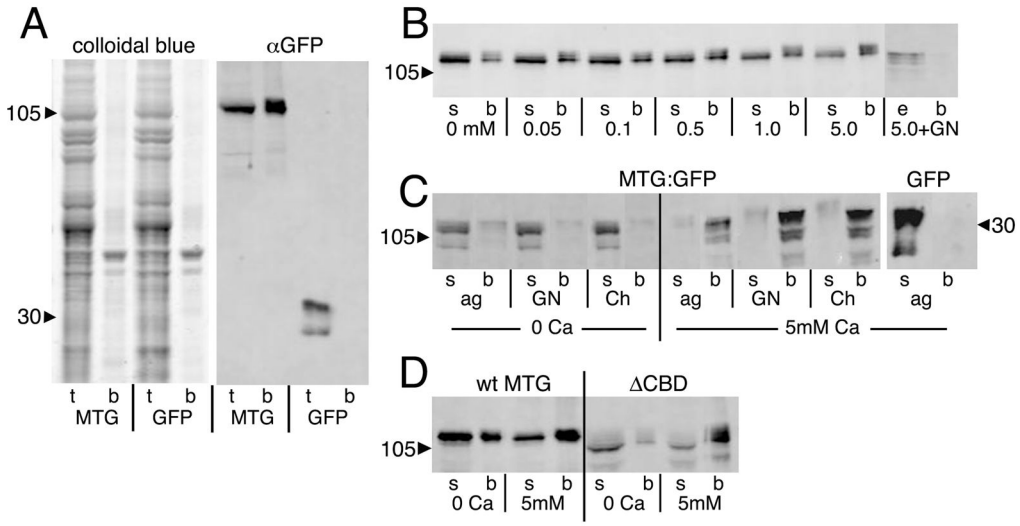

Fig 7. MTG binds to N-acetylglucosamine (GlcNAc) in a Ca^{2+}-dependent manner

Salivary gland lysates from wandering 3rd instar animals expressing either MTG::GFP or GFP alone assayed on GlcNAc-conjugated agarose beads. **(A)** Representative Western Blots of total lysate (t) and bead-bound proteins (b) separated by SDS-PAGE. Total protein (left panel) shows MTG::GFP enrichment of a small subset of proteins. Anti-GFP (right panel) shows MTG::GFP bound to beads, while GFP is found only in the lysate. **(B)** MTG::GFP binding is Ca^{2+}-dependent, and competed by GlcNAc. The supernatant (s) is the lysate after incubation on beads. The bead fraction (b) is protein bound to beads. The eluate (e) is protein released from beads by 0.4M GlcNAc wash. Numbers refer to Ca^{2+} concentration in μM. **(C)** MTG::GFP binds GlcNAc (GN), GlcNAc polymer Chitin (Ch) and agarose (ag) in a Ca^{2+}-dependent manner. GFP does not bind under any conditions (agarose shown). **(D)** ΔCBD also shows Ca^{2+}-dependent binding of GlcNAc. Arrowheads indicate protein molecular weight in kDa.

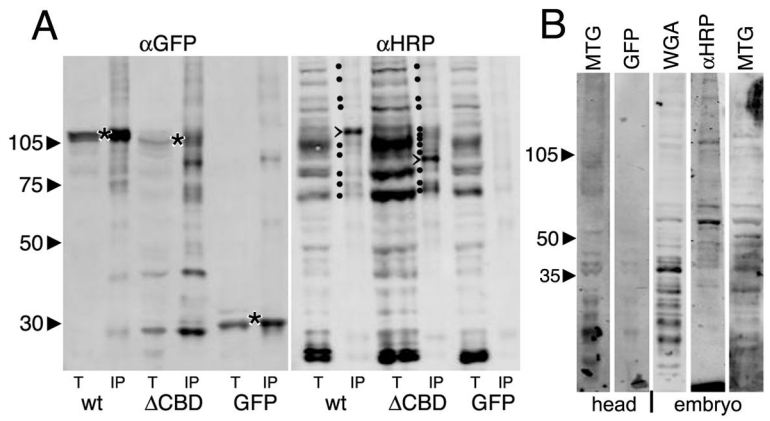

Fig 8. Both wildtype and ΔCBD MTG bind HRP-epitope glycoproteins

(A) Representative Western Blots of total lysate (t) or immunoprecipitate (IP) from wandering 3rd instar salivary gland lysates. Wildtype (wt) MTG::GFP, ΔCBD MTG::GFP and GFP alone were IP isolated using anti-GFP (left), and probed with α-HRP (right). Left (αGFP): all three proteins are pulled down (*). The ΔCBD protein is slightly smaller than wt protein, as expected. Right: (α-HRP): The total lysates show multiple bands, with a few bands (marked with dots) pulled down by wildtype MTG::GFP. One major band migrates at ~115 kDa. ΔCBD pulls down more HRP epitope proteins, with a major band at ~94 kDa (major bands are marked with >). **(B)** Using MTG::GFP as a probe in a Far-Western Blot, wandering 3rd instar salivary gland lysates from animals expressing MTG::GFP, or GFP alone, were applied to membranes blotted with proteins of head tissue (2 lanes, left) or embryos (3 lanes, right). GFP alone shows no consistent binding to any protein bands, whereas MTG::GFP consistently binds many protein bands. αHRP antibody and WGA lectin recognize similar glycoproteins.